Crack nucleation and growth in α/β titanium alloy with lamellar microstructure under uniaxial tension: 3D X-ray tomography analysis

N. Dang, L. Liu, J. Adrien, S. Cazottes, W. Xiao, C. Ma, L. Zhou, E. Maire

Crack nucleation and growth in α/β titanium alloy with lamellar microstructure under uniaxial tension: 3D X-ray tomography analysis

Author: Ning DANG[a,b], Lingyu LIU[c], Jérôme ADRIEN[b], Sophie CAZOTTES[b], Wenlong XIAO*[,a], Chaoli MA[a], Lian ZHOU[d], Eric MAIRE*[,b]

[a] *Key Laboratory of Aerospace Advanced Materials and Performance of Ministry of Education, School of Materials Science and Engineering, Beihang University, Beijing 100191, China*
[b] *Université de Lyon , INSA de Lyon, MATEIS CNRS-UMR 5510, F-69621 Villeurbanne, France*
[c] *Baoti Group Co., Ltd., Baoji, 721014, China*
[d] *Northwest Institute for Nonferrous Metal Research, Xi'an 710016, China*

Abstract: *In situ* tensile tests were carried out on notch axisymmetric samples of as-cast (α+β) Ti alloy to analyze evolution of void/micro-crack with the help of X-ray Synchrotron tomography. The results indicate that junctions or boundaries of α colonies could be the most vulnerable sites for voids nucleation. In addition, during the growth and coalescence procedure, "ligaments" could be observed on the voids/micro-crack. A "bypassing & fracture" propagating approach was proposed and validated to interpret the existence of "ligaments". In the propagating procedure, due to lacking of hard precipitations, microstructure zone and other inserting colony could play a role as hard obstacle in the growing path. This could induce a "bypassing & fracture" propagating approach for void coalescence and micro-crack growth.

Keywords: Ti-6Al-4V alloy; X-ray tomography; *in situ* tensile test; void propagation; bypassing behavior

*Corresponding author.
E-mail: eric.maire@insa-lyon.fr (Eric MAIRE);
wlxiao@buaa.edu.cn (Wenlong XIAO)

The Ti-6Al-4V(wt%, hereafter named TA6V) titanium alloys, which consists of HCP α phase and BCC β phase ,are widely used in modern industries, especially in advanced aerospace field because of their low density, high specific strength and excellent corrosion resistance [1-3]. As for TA6V casting components, because of relatively slow cooling rate from β phase field, only full lamellar structure could exist at ambient temperature. Therefore, in order to enhance the properties of the components, it is desirable to analyze the damage development in TA6V alloys with such a lamellar structure.

Generally, the damage evolution for metals includes the nucleation, growth and coalescence of small internal voids. As early as 1960s, several models were proposed to describe the growth of voids [4,5]. Advanced damage models were then established to interpret the whole damage procedure[6,7]. Recently, the development of X-ray computed tomography technology (XCT) has facilitated the tracking of initiation and growth of the voids [8-10]. S. Singh *et al.* have proved that the discontinuous surface cracks are actually a continuous and tortuous crack with the help of 3D Synchrotron X-ray CT[8].By combining the results from XCT and finite element method (FEM), E. Maire *et al.* have analyzed ductile damage processing of dual phase steel[11-14], aluminum alloys[15-17] and titanium alloys[18-19]. In these papers, the influence of variation in stress triaxiality on damage procedure has been taken into account by performing in-situ tensile tests [11-14,16,18-19]; however, post-mortem analysis was performed on the basis of Solid Mechanics rather than Material Science, which may disregard the role of microstructure morphologies playing in damage development.

With respect to titanium alloys, there have been several attempts in the literature to analyze the damage development with the help of X-ray tomography. However, Most of the attention was attracted on propagation of crack in fatigue test[20-27] rather than in uniaxial tensile test[18,19,28]. Thanks to diffraction and phase-contrast X-ray tomography, M. Herbig *et al.* [22]could analyze the local crack growth rate of short fatigue cracks and crystallographic orientation of fracture surface for β-21S titanium alloy in three dimensions. L.Lecarme *et al* [18] could reveal heterogeneous void growth of Ti-6Al-4V titanium alloy with the help of in-situ 3D X-ray

tomography combining automatic cavity tracking.

Recently, as microstructure morphology can play a significant role in damage development of Ti alloys, plenty of researchers focus on the damage behavior of Ti alloys with different microstructure morphologies, such as fully equiaxed [18, 22,27-30] or bimodal morphologies[21,25]. But less attention was paid on damage development of Ti alloy with fully lamellar microstructure morphology[19,31,32]. C.S.Tan *et al.* have compared crack expanding path and fatigue life of TC21 titanium alloys with equiaxed microstructure and full lamellar microstructure[31]. Because of considerable discrepancy in α phase morphologies, they showed significant difference in void coalescence and micro-crack formation. Furthermore, the role of primary α phase played in crack initiation and propagation was indicated by analyzing the interaction between void development and α phase[32]. M. Pushkareva *et al* [19] have analyzed the void growth of pure titanium with lamellar microstructure during tensile deformation by in-situ X-ray tomography. Grain orientation can affect void growth stronger than intervoid spacing and material strength, which was evidenced by crystal plasticity simulating results [19].

Whereas, there is still lack of sufficient work on damage behavior of Ti alloys with fully lamellar microstructure, especially for damage evolution during uniaxial tensile deformation. Therefore, in this current work, we have analyzed the voids coalescence and micro-crack growth of lamellar structured TA6V alloy. We were able to indicate the preferable nucleating site of voids by *in situ* 3D micro-tomography. Besides, during the growing procedure of voids/micro-crack, a “bypassing” behavior was proposed in the damage analysis of Ti alloy and validated by the existence of “ligaments” between the two lips of the voids/micro-crack.

2. Experiments

A TA6V plate, with a dimension of 300mm×200mm×10mm, was prepared by casting. The chemical composition of as-received TA6V plate consists of 6.43Al,

4.21V, 0.40Fe, 0.15Si, 0.10C, 0.05N,0.015H and bal. Ti(wt.%). The subsequent heat treatment parameters depend on the β-transus temperature, which is 995℃±5℃[1]. On the basis of indications from Ref.[1][33，34], heat treatment should be performed in (α+β) phase field in order to obtain fully lamellar structure. Thus, the TA6V plate was solution treated at 960℃ for 1 hour followed by air cooling, and then aged at 540℃ for 8 hours to ensure the formation of fully lamellar microstructure and equilibrium distribution of α/β phase (See OM images in Fig.1).

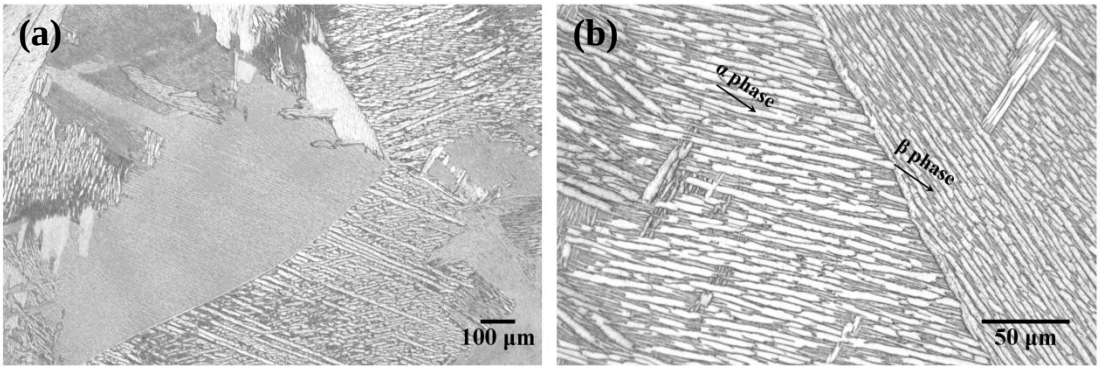

Fig.1. Microstructure morphology of TA6V alloys before deformation imaged by Optical Microscopy(OM);(a) low magnification,(b) high magnification (α phase in bright, and β phase in dark)

Subsequently, TA6V specimens with a size of 35mm×10mm×10mm were cut from the plate for machining cylindrical pre-samples for in-situ tensile test. Notched axis symmetric samples were then manufactured from these cylinders. The geometry of the test samples is given in Fig. 2.

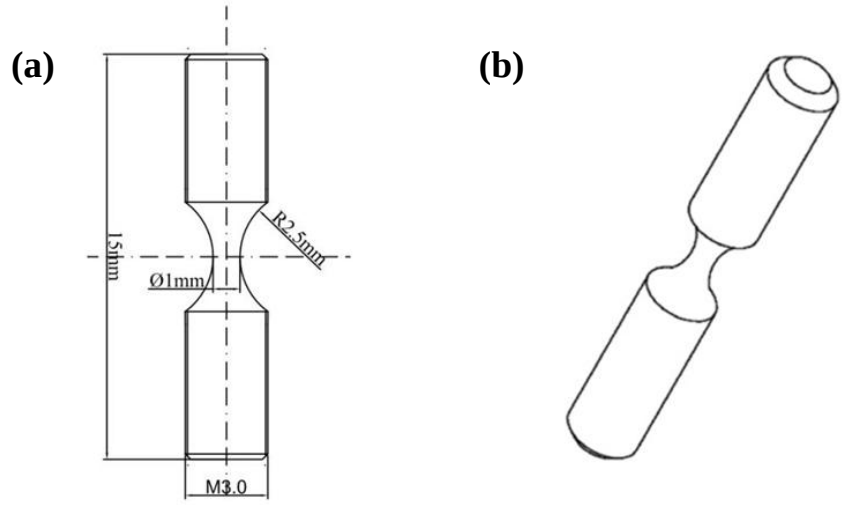

Fig.2. Geometry of sample for in-situ tensile test in (a) and 3D view of the sample in (b) [12].

The local strain ε_{local} at each step was calculated as follows,

$$\varepsilon = \ln\left(\frac{S_0}{S}\right) \quad (1)$$

where S_0 is the area of initial cross-section before deformation, and S is the solid area of minimal cross-section at each damage step，which means that in the measurement of S, the eventual area of the voids in the current section should be subtracted. The minimal cross-section S was also used to evaluate the true stress in this section,

$$\sigma_{true} = \frac{F}{S} \quad (2)$$

where F is the measured force during the tensile test. The calculated results are presented in Fig.2(b).

The damage evolution during in-situ tensile test was monitored by using a high resolution X-ray micro tomography equipment located at the European Synchrotron Radiation Facility(ESRF, ID19 beam line) in Grenoble, France. The samples were deformed by a dedicated tensile machine mounted on the rotation stage which can rotate at a constant speed during data acquisition[35,36]. The following experimental parameters were used in this study: a beam energy of 40 keV was used to acquire 1200 radiographies from 0 ° to 180 ° for the tomographic reconstruction; and time for recording one radiography was set to 180ms. The acquisition time for one scan (including scanning data acquisition and saving on the hard disk) was below 10 min. More details concerning set-up of tomography and the dedicated in-situ tensile rig

used in this study can be found elsewhere [11, 35-36]. Only central area in the minimum section of test samples was imaged, and the voxel size was 1.3×1.3×1.3 μm^3. The reconstruction of the volumes was achieved by using *PyHST* [http://ftp.esrf.fr/scisoft/PYHST2/], a dedicated Python software available at ESRF.

Before the test, initial scan was performed to obtain the original state of the sample. Subsequently, several scans were performed until the sample fractured. Within the elastic deformation period, the loading rate was set to 5μm/s; when the sample started to yield, the loading rate was decreased to 0.1μm /s in order to obtain more scans during the deformation. During the tomographic scan, loading was stopped but not released; and the sample was maintained at a fixed position. In Ref.[13,15], it was proved that the step-by-step procedure implemented in this work could give quantitative results similar to the results obtained by continuous loading procedure.

The post treatment and 3D rendering work was managed by using open source image analysis software, *Image J*[37] with plugin *3D viewer*[38]. In the image processing procedure, one java script macro that attached to *Image J* was written to carry out the reconstruction operations (including creating image stacks, thresholding the stack to obtain a binary image with matrix and voids, and visualizing the reconstructed volumes). It is worth to note that in order to focus on the voids/crack, the matrix of the material was set transparent. In other words, only the voids/crack are presented in the 3D reconstructed volume.

Then, after tensile testing, the samples were embedded into epoxy matrix, followed by a standard metallographic polishing step, down to the central plane of the sample. In the final polishing step, a vibratory polisher with a mixed solution of OP-S and H_2O_2 was used for 2.5 hours in order to achieve a mirror finish. Subsequent etching processing was performed by Kroll's reagent (1 ml HF+ 3ml HNO_3+ 96ml water). The tensile axis was included in the so obtained polished section. The microstructure morphology, as well as the voids, was observed by using Zeiss Supra 55VP scanning electron microscope (SEM).

3. Results and Discussion

As shown by load/displacement curve recorded during the test (see Fig.3(a)), 8 scans(excluding the initial scan before deformation) with different plastic strain were acquired during the plastic deformation(until the sample failed). The true stress and local true strain of these different step are marked by red points in Fig.3(b). As shown in Fig.3(a), the first scan (step 1) was performed at around the yielding point; and the final scan(step 8) was finished just before fracture. From Fig.3, it can be rational deducted that no obvious work hardening could occur during the plastic deformation.

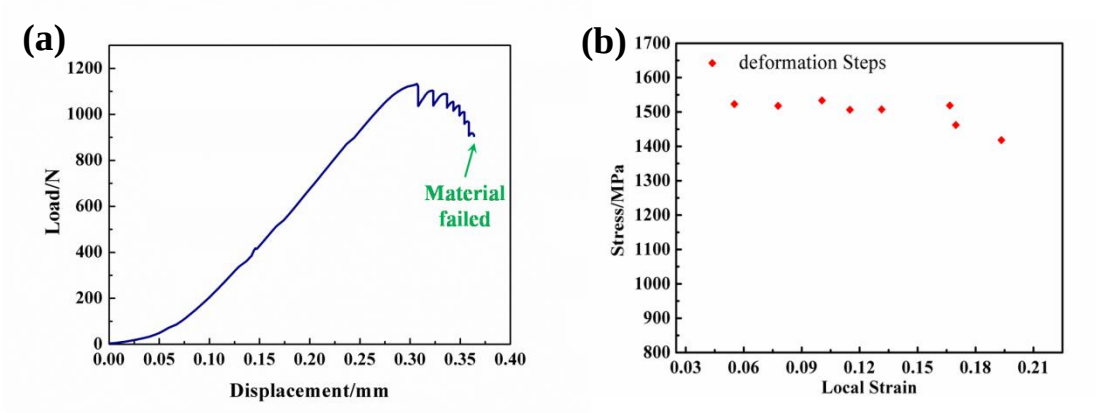

Fig.3. Load-displacement curve in (a) and true Stress-Local Strain scatter diagram for scanning area in (b).

Fig.4 depicts reconstructed tomographic slices which were extracted from the tomographic 3D block at tensile state of just yielding (Step 1), intermediate deformation (Step 5), and just before fracture (Step 8), respectively. These slices are oriented parallel to the tensile direction, which is vertical in these grey level images. In addition, void(dark part inside the sample) exists near the center of the sample, which means that stress concentrates in the center of the sample.

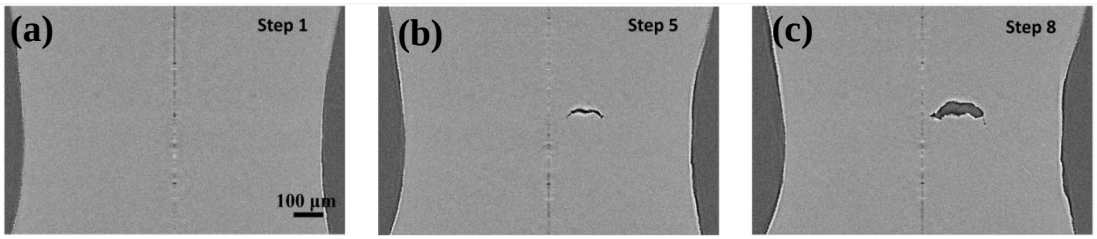

Fig.4. The reconstructed tomographic slices parallel to the tensile axis at step 1, 5 and 8.

Fig. 5 shows the typical evolution of a reconstructed 3D image of the sample. In order to focus on the voids/crack, the matrix of materials was set transparent for this 3D rendering. The voids and micro-crack are set as a fully opaque yellow surface. These 3D sub-regions were extracted from the tomographic work at different tensile steps. The vertical direction of the sections is parallel to the tensile axis. Voids, in the form of micro-cracks, can be observed at just beginning of plastic deformation (Fig. 5(a)). The micro-cracks coalesce to form larger cracks near the center of the sample, as shown in Fig.5 (b) and (c). These larger cracks seem to be inclined when comparing with the tensile axis.

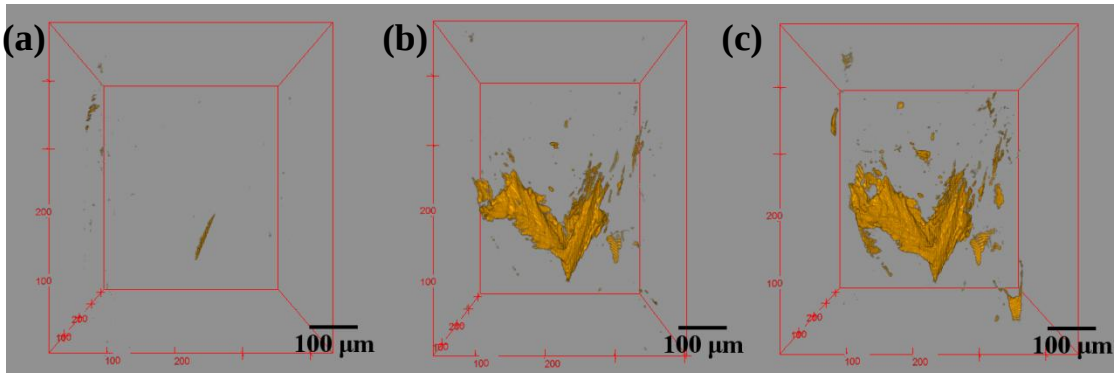

Fig.5. Volume rendering of voids/micro-cracks in (a) Step1, (b) Step7 and (c) Step8.. The dimension of the reconstructed block is 585×585×650 μm^3. For interpretation of the references to colour in this figure legend, the reader is referred to the web version of this article.

Fig.5 shows the profile evolution of one particularly targeted void (yellow part in the image, named void A) in different deformation steps, which has the largest volume and leads to final rupture. This image was obtained by cropping the reconstructed

volumes in order to focus on the details. Note that the perspective view makes the insertion of a scale bar inappropriate; but the dimension of the X dimension of the box is given in each figure. The void A initiated just after yielding(Step 1), which has a “shuttle-like” morphology with some ledges located at the edge(Fig. 5(a)).Before the occurrence of void coalescence(Step 5), it is considered as a tiny, and its evolution with increasing plastic strain is visible in Steps 2 and 3 (Fig.6(b)-(c)). The void A gradually develops into a larger micro-crack with further deformation. As seen from Fig. 6(d)-(f), void A and two other voids coalesced to form a coherent main crack(marked as M crack in this work),leading to final fracture.

It is worth noticing in Fig.6(a) that some “holes” (matrix ligaments) are visible inside the tiny crack (void A), as selected by blue circles. As the matrix of material is transparent, such “holes” in void A could be referred to the fact that the solid titanium could still exist in some local parts. In other words, these “holes” actually represent “*ligaments*” of solid Ti alloy during void evolution (For interpretation of the relationship between the tiny crack (void A) and “holes” (*ligaments*), more details can be found in the appendix of this article.). It is also interesting to note that same phenomenon can also be visible in other steps of damage evolution. Even after coalescence, the “*ligaments”* still exist in some parts of M crack.

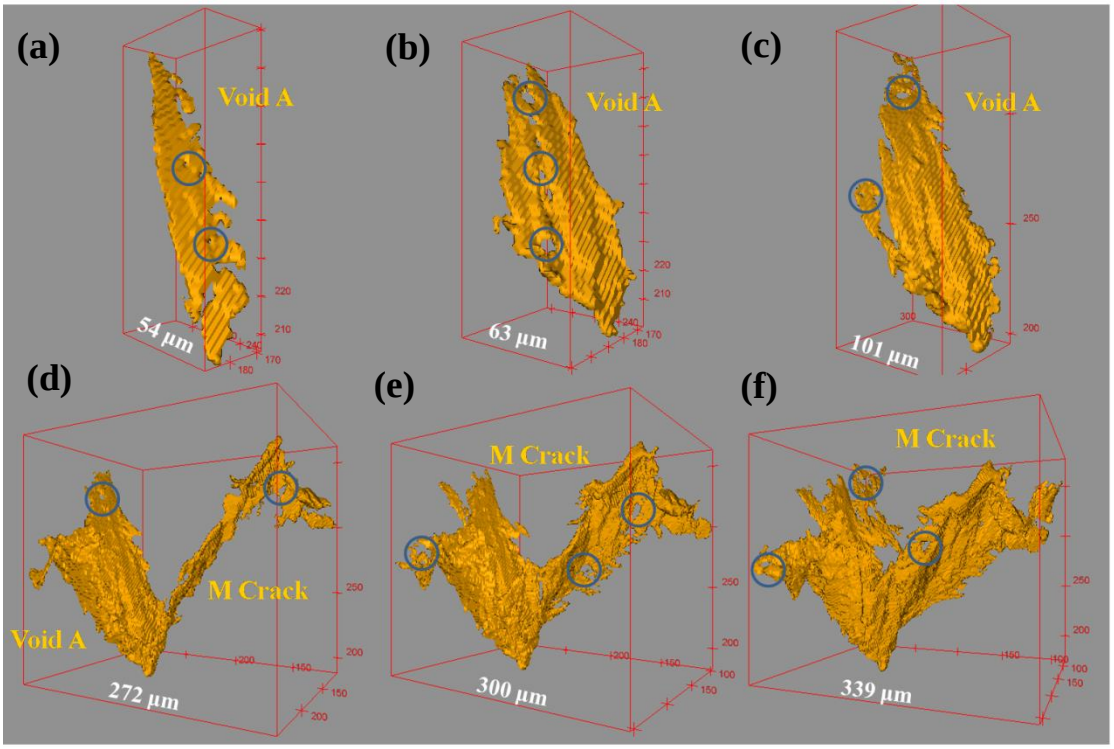

Fig.6. Volume rendering of a targeted void in different damage steps; before coalescence in (a) Step1,(b) Step2,(c) Step3; after coalescence (treated as M crack) in (d) Step5, (e) Step 6, (f) Step7. The solid material was set as transparent matrix in order that yellow part can reflect the aspect of voids/crack; blue circles marked the "holes" (ligaments) observed within Void A and M crack.

To deepen the investigation of damage behavior, one region below the fracture surface was selected for SEM observation (see Fig.7). It can be noticed that the sample still keeps a fully lamellar structure with the thickness of α laths in the range of 2~4 μm, although this local region may experience severe plastic deformation.

From Fig.7(a), it can be seen that the junctions between two or three colonies are more prone to be nucleating sites for voids. Fig.7(b)&(c) present the micro-voids indicated in Fig.7(a) in a higher magnification. The size of these voids is about 1μm, which is smaller than the thickness of α lath (2~4μm). Due to stress concentration, voids tend to initiate at boundaries or junction of the colonies. Moreover, as shown in Fig.7(d),which was the selected zone marked by red rectangle, voids tend to grow along the boundaries between two adjacent colonies(pointed out by black arrows).

As indicated by Ref.[1,2], for Ti alloy with fully lamellar microstructure morphology,

within one α colony, all the α laths tend to be parallel to each other and exhibit almost the same crystallographic orientation. In other words, neighboring colonies may have distinct misorientation, which may promote the nucleation of voids at the boundaries and the junctions. The growing path of the voids may follow the boundaries of this neighboring α colonies (see Fig.7(d)).

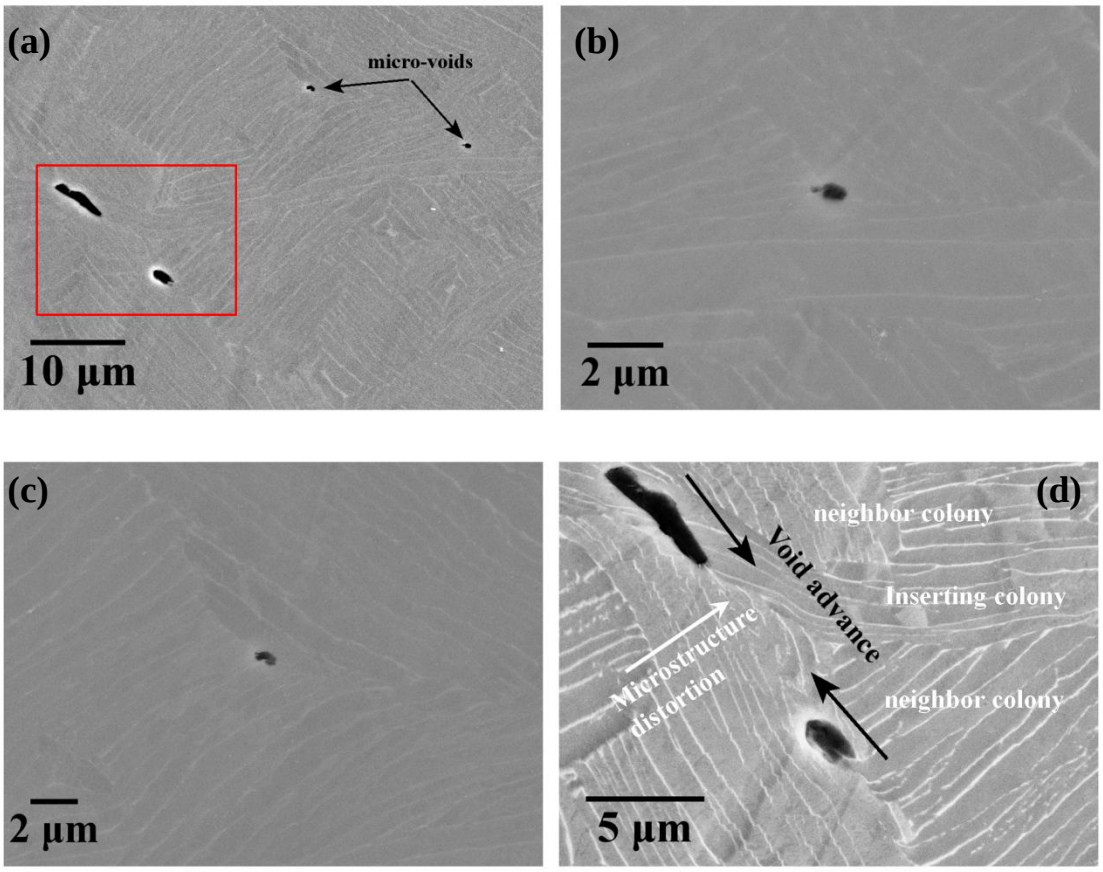

Fig.7. (a) microstructure morphology and voids distribution for the region in central plane of in situ tensile sample; (b)(c) shows aspect of micro-voids selecting in (a); (d)high magnification of selecting zone in(a), The tensile direction is parallel to horizontal.

According to the knowledge about failure of metallic materials under monotonic loadings, commonly, coalescence was assumed to occur when the materials ligament between the neighboring voids was exhausted [39-41], so that the neighboring voids can merge. In this current work, neighboring voids can contact each other; however, the material ligaments between these voids may still exist in some local regions (see the "*holes*" marked by blue circles in Fig.6). These "*ligaments*" inside the void A or

M crack can be observed in each step of damage evolution, even in the period of main crack(M Crack) nucleation and propagation (Fig.6(d)-(f)). It is then certainly an important feature of void/crack propagation.

Besides, Fig.6 also depicts that the position and number of "*ligaments*" may vary in each step of damage development. Within one step of damage evolution, former "*ligaments*" may annihilate and new ones may form (See Fig.6(a),(b)and (c)). This phenomenon was previously reported in metal matrix composites or hard precipitates inserted in soft matrix [42-46]. The region where solid material still exists in the void or micro-crack, was reflected in terms of vacancy loops at the interface between soft-hard phases.

As presented in Fig.6, the appearance and disappearance of "*ligaments*" (marked by blue circles) could verify this propagating procedure of voids for TA6V alloy. While in this current work, no hard particles or precipitations can be found. Thus, probably other features could play a role as "hard particles" or "hard precipitations" during damage evolution. From Fig.7(d), it can be seen that in the growing path of voids, microstructure distortion could be found, which may result from heterogeneous deformation and lead to stress concentration. In addition, one colony, which exhibit distinct misorientations with its neighbors, inserts in the growing path of voids. Voids may bifurcate when meeting this inserting colony. Therefore, this colony and microstructure distorting zone may be considered as "hard particles" in this work.

Fig.8 gives another evidence to demonstrate this "*bypassing*" procedure. As shown in Fig.8, the initiation of micro-crack could result from the coalescence of two void sites (marked VS1 and VS2), which may nucleate at the boundary of colonies AC1 and AC2, and the junction of AC3 and AC4, respectively. Because of distinct misorientation with neighbor colonies and microstructure distortion, colony AC3(treated as inserting colony) and local distorting zone could be treated as "hard" obstacles, in which the "*bypassing*" procedure may occur(just broken ligaments can be seen in the region, indicated by green rectangle).

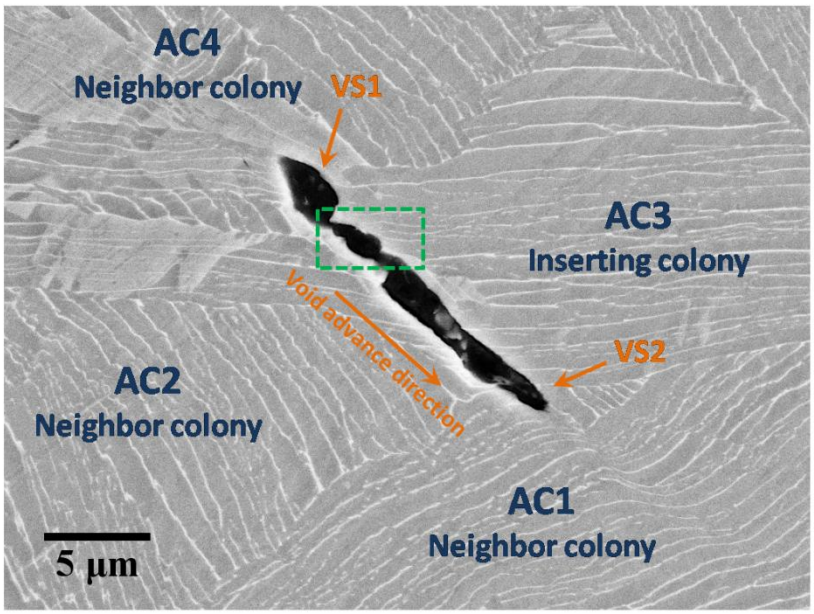

Fig.8. micro-crack propagation in terms of "*bypassing*" procedure revealed by SEM

4. Conclusions

In summary, micro-crack initiation and growth in the TA6V alloy with lamellar microstructure during tensile deformation was tracked and analyzed based on X-ray tomography and post mortem SEM. It shows that the junctions α colonies are the preferential sites for nucleation of tiny micro-cracks. The boundaries of respecting α colonies might be the potential path for propagation.

During growth of micro-crack, ligaments of unbroken Ti material can be noticed. It is certainly an important characteristic of crack propagation for Ti alloy. The grown micro-cracks can be treated as "bridges" at the edge by such ligaments. We suggest microstructure distorting zone or "inserting colony" could act as "hard" obstacles to inhibit the advance of crack in the growing path. Then the void could bypass such "hard" obstacle to contact its neighboring void instead of fracturing it, symbolized by the appearance of ligaments in 3D reconstructed volume. Finally, the hard obstacle fractured to form micro-crack completely, and the micro-crack could continue to propagate along the former growing direction.

Acknowledgement

The authors are grateful to the financial support by International Science and Technology Cooperation Program of China (2015DFA51430), National Natural Science Foundation of China (NSFC, No. 51671012) and Aeronautical Science Foundation of China (2015ZF51069) and to carry out this work. Ning DANG would like to thank the China Scholarship Council (File No. 201406020005) for financial support. Beamtime allocated by the ESRF on the ID19 beam-line through long term project is also acknowledged.

Data availability

The raw/processed data required to reproduce these findings cannot be shared at this time as the data also forms part of an ongoing study.

Appendix A: The interpretation of relationship between the tiny crack(void A) and the “holes”(ligaments) on this crack, taking step 2 as an example.

The “holes” in the crack(void A) was used to verify the existence of material ligaments during the propagation of crack. Furthermore, these “holes” could be treated as evidence to prove that damage could evolve in approach of “bypassing & fracture”. In order to describe the relationship between the crack (void A) and “holes”(ligament), the 3D bloc of step 2 was selected as a classical example to present the Void A and “holes”(See Fig.A1).

As shown in Fig. A1(a), one crack(void A) can be observed within the solid material which was set as transparent matrix. One block was created by yellow cube,

including void A and the solid material around it. In Fig.A1 (b), the solid material was set as dark matrix, while void A as bright part. It can be clearly seen that some black “holes” (indicated by blue arrows) exist in the bright part (void A), which means TA6V material ligaments exist in this local region (black “holes” positions).

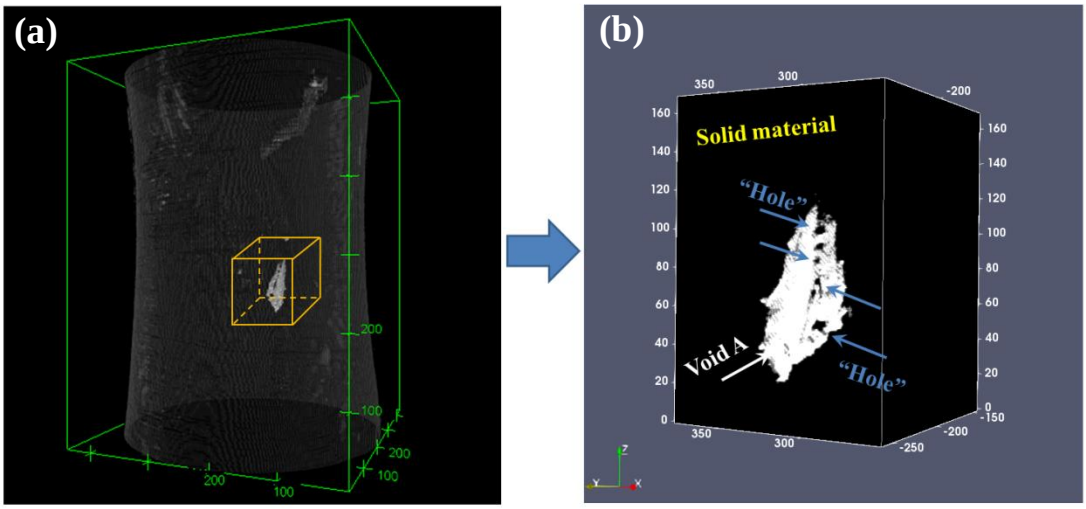

Fig.A1. 3D views of volume obtained by tomography: (a) whole sample in Step 2, (b) selected cube block in (a). The perspective view makes the insertion of a scale bar inappropriate. The dimension of the reconstructed block is 585×585×650 μm^3 in (a) and in (b) 156×126×222 μm^3.

Furthermore, in other steps of the damage procedure, “holes” (material ligaments) can also be found in the void or main crack (see Fig.6, marked by blue circles) but with different numbers and the positions; in other words, materials ligaments can exist in all the steps of damage development.

References

[1] M. Peters, J. Kumpfert, C.H. Ward, C. Leyens, Titanium Alloys for Aerospace Applications, Titanium and Titanium Alloys, Wiley-VCH Verlag GmbH & Co. KGaA, 2005, pp. 333-350.
[2] R. Boyer, G. Welsch, E.W. Collings, Materials Properties Handbook: Titanium Alloys, ASM International, 1994.
[3] M.T. Jia, D.L. Zhang, B. Gabbitas, J.M. Liang, C. Kong, A novel Ti–6Al–4V alloy microstructure with very high strength and good ductility, Scripta Mater. 107 (2015) 10-13.

[4] F.A. McClintock, A Criterion for Ductile Fracture by the Growth of Holes, J. Appl. Mech. 35 (1968) 363-371.
[5] J.R. Rice, D.M. Tracey, On the ductile enlargement of voids in triaxial stress fields, J. Mech. Phys. of Solids. 17 (1969) 201-217.
[6] A.A. Benzerga, J.-B. Leblond, Ductile Fracture by Void Growth to Coalescence, in: H. Aref, E.v.d. Giessen (Eds.) Advances in Applied Mechanics, Elsevier, 2010, pp. 169-305.
[7] T. Pardoen, F. Scheyvaerts, A. Simar, C. Tekoğlu, P.R. Onck, Multiscale modeling of ductile failure in metallic alloys, C.R. Phys. 11 (2010) 326-345.
[8] S.S. Singh, J.J. Williams, M.F. Lin, X. Xiao, F.D. Carlo, N. Chawla, In Situ Investigation of High Humidity Stress Corrosion Cracking of 7075 Aluminum Alloy by Three-Dimensional (3D) X-ray Synchrotron Tomography, Mater. Res. Lett. 2 (2014) 217-220.
[9] S.R. Stock, Microtomography of materials, Int. Mater. Rev., 44 (1999) 141-164.
[10] E. Maire, P.J. Withers, Quantitative X-ray tomography, Int. Mater. Rev., 59 (2014) 1-43.
[11] E. Maire, O. Bouaziz, M. Di Michiel, C. Verdu, Initiation and growth of damage in a dual-phase steel observed by X-ray microtomography, Acta Mater. 56 (2008) 4954-4964.
[12] C. Landron, O. Bouaziz, E. Maire, J. Adrien, Characterization and modeling of void nucleation by interface decohesion in dual phase steels, Scripta Mater. 63 (2010) 973-976.
[13] C. Landron, E. Maire, O. Bouaziz, J. Adrien, L. Lecarme, A. Bareggi, Validation of void growth models using X-ray microtomography characterization of damage in dual phase steels, Acta Mater. 59 (2011) 7564-7573.
[14] G. Requena, E. Maire, C. Leguen, S. Thuillier, Separation of nucleation and growth of voids during tensile deformation of a dual phase steel using synchrotron microtomography, Mater. Sci .Eng. A. 589 (2014) 242-251.
[15] E. Maire, J.C. Grenier, D. Daniel, A. Baldacci, H. Klocker, A. Bigot, Quantitative 3D characterization of intermetallic phases in an Al-Mg industrial alloy by X-ray microtomography, Scripta Mater. 55 (2006) 123-126.
[16] S. Thuillier, E. Maire, M. Brunet, Ductile damage in aluminium alloy thin sheets: Correlation between micro-tomography observations and mechanical modeling, Mat. Sci. Eng. A. 558 (2012) 217-225.
[17] R. Fernández Gutiérrez, F. Sket, E. Maire, F. Wilde, E. Boller, G. Requena, Effect of solution heat treatment on microstructure and damage accumulation in cast Al-Cu alloys, J. Alloys and Compds. 697 (2017) 341-352.
[18] L. Lecarme, E. Maire, K.C.A. Kumar, C. De Vleeschouwer, L. Jacques, A. Simar, T. Pardoen, Heterogenous void growth revealed by in situ 3-D X-ray microtomography using automatic cavity tracking, Acta Mater. 63 (2014) 130-139.
[19] M. Pushkareva, J. Adrien, E. Maire, J. Segurado, J. Llorca, A. Weck, Three-dimensional investigation of grain orientation effects on void growth in commercially pure titanium, Mater.Sci. Eng. A. 671 (2016) 221-232.

[20] S. Birosca, J.Y. Buffiere, F.A. Garcia-Pastor, M. Karadge, L. Babout, M. Preuss, Three-dimensional characterization of fatigue cracks in Ti-6246 using X-ray tomography and electron backscatter diffraction, Acta Mater. 57(19) (2009) 5834-5847.
[21] S. Birosca, J.Y. Buffiere, M. Karadge, M. Preuss, 3-D observations of short fatigue crack interaction with la2mellar and duplex microstructures in a two-phase titanium alloy, Acta Mater.

59(4) (2011) 1510-1522.
[22] M. Herbig, A. King, P. Reischig, H. Proudhon, E.M. Lauridsen, J. Marrow, J.-Y. Buffière, W. Ludwig, 3-D growth of a short fatigue crack within a polycrystalline microstructure studied using combined diffraction and phase-contrast X-ray tomography, Acta Mater. 59(2) (2011) 590-601.
[23] L. Babout, Ł. Jopek, M. Preuss, 3D characterization of trans- and inter-lamellar fatigue crack in (α+β) Ti alloy, Mater. Charact. 98 (2014) 130-139.
[24] D. Shiozawa, Y. Nakai, T. Murakami, H. Nosho, Observation of 3D shape and propagation mode transition of fatigue cracks in Ti–6Al–4V under cyclic torsion using CT imaging with ultra-bright synchrotron radiation, Int. J. Fatigue 58 (2014) 158-165.
[25] T.P. Chapman, K.M. Kareh, M. Knop, T. Connolley, P.D. Lee, M.A. Azeem, D. Rugg, T.C. Lindley, D. Dye, Characterisation of short fatigue cracks in titanium alloy IMI 834 using X-ray microtomography, Acta Mater. 99 (2015) 49-62.
[26] J. Kar, D. Chakrabarti, S.K. Roy, G.G. Roy, Beam oscillation, porosity formation and fatigue properties of electron beam welded Ti-6Al-4V alloy, J. Mater. Process. Tech. 266 (2019) 165-172.
[27] T. Persenot, A. Burr, G. Martin, J.-Y. Buffiere, R. Dendievel, E. Maire, Effect of build orientation on the fatigue properties of as-built Electron Beam Melted Ti-6Al-4V alloy, Int. J. Fatigue 118 (2019) 65-76.
[28] M. Preuss, P.J. Withers, E. Maire, J.Y. Buffiere, SiC single fibre full-fragmentation during straining in a Ti–6Al–4V matrix studied by synchrotron X-rays, Acta Mater. 50(12) (2002) 3177-3192.
[29] G. Li, R. Shi, Q. Fan, Y. Xia, H. Zhang, Three-dimensional microstructure-based micromechanical modeling for TC6 titanium alloy, Mater. Sci. Eng. A 685 (2017) 327-331.
[30] J. Tan, L. Lu, H.Y. Li, X.H. Xiao, Z. Li, S.N. Luo, Anisotropic deformation and damage of dual-phase Ti-6Al-4V under high strain rate loading, Mater. Sci. Eng. A 742 (2019) 532-539.

[31] C. Tan, X. Li, Q. Sun, L. Xiao, Y. Zhao, J. Sun, Effect of α-phase morphology on low-cycle fatigue behavior of TC21 alloy, Int. J. Fatigue. 75 (2015) 1-9.
[32] C. Tan, Q. Sun, L. Xiao, Y. Zhao, J. Sun, Cyclic Deformation and Microcrack Initiation During Stress Controlled High Cycle Fatigue of a Titanium Alloy, Mater. Sci. Eng. A.711 (2017)212-222.

[33] R. Ding, Z.X. Guo, A. Wilson, Microstructural evolution of a Ti–6Al–4V alloy during thermomechanical processing, Mater. Sci. Eng. A. 327(2) (2002) 233-245.
[34] S.L. Semiatin, S.L. Knisley, P.N. Fagin, D.R. Barker, F. Zhang, Microstructure evolution during alpha-beta heat treatment of Ti-6Al-4V, Metall and Mat Trans A 34(10) (2003) 2377-2386.

[35] M.D. Michiel, J.M. Merino, D. Fernandez-Carreiras, T. Buslaps, V. Honkimäki, P. Falus, T. Martins, O. Svensson, Fast microtomography using high energy synchrotron radiation, Rev. Sci. Instrum. 76 (2005) 043702-043702-043707.
[36] J.Y. Buffiere, E. Maire, J. Adrien, J.P. Masse, E. Boller, In Situ Experiments with X ray Tomography: an Attractive Tool for Experimental Mechanics, Exp. Mech. 50 (2010) 289-305.
[37] C.T. Rueden, J. Schindelin, M.C. Hiner, B.E. DeZonia, A.E. Walter, E.T. Arena, K.W. Eliceiri, BMC Bioinformatics, 18 (2017) 529.
[38] B. Schmid, J. Schindelin, A. Cardona, M. Longair, M. Heisenberg, BMC Bioinformatics, 11

(2010) 274.
[39] A. Pineau, A.A. Benzerga, T. Pardoen, Failure of metals I: Brittle and ductile fracture, Acta Mater. 107 (2016) 424-483.
[40] P.D. Nicolaou, S.L. Semiatin, An analysis of the effect of continuous nucleation and coalescence on cavitation during hot tension testing, Acta Mater. 48 (2000) 3441-3450.
[41] C.H. Caceres, D.S. Wilkinson, Large Strain Behavior of a Superplastic Copper Alloy—II: Cavitation and Fracture, Acta Metall. 32 (1984) 423-434.
[42] B. Marino, F. Mudry, A. Pineau, Experimental study of cavity growth in ductile rupture, Eng. Frac. Mech.22 (1985) 989-996.
[43] L. Babout, Y. Brechet, E. Maire, R. Fougères, On the competition between particle fracture and particle decohesion in metal matrix composites, Acta Mater. 52 (2004) 4517-4525.
[44] M.F. Ashby, Work hardening of dispersion-hardened crystals, Phil. Mag. 14 (1966) 1157-1178.
[45] M.F. Horstemeyer, A.M. Gokhale, A void–crack nucleation model for ductile metals, Int J Solids Struct, 36 (1999) 5029-5055.
[46] L. Babout, E. Maire, R. Fougeres, Damage initiation in model metallic materials: X-ray tomography and modelling, Acta Mater. 52 (2004) 2475-2487.